Journal of Alloys and Compounds 484 (2009) 90–94

Contents lists available at ScienceDirect

Journal of Alloys and Compounds

journal homepage: www.elsevier.com/locate/jallcom

Formation mechanisms of precipitates in an Al–Cu–Li–Zr alloy and their effects on strength and electrical resistance of the alloy

S. Ahmadi [a,*], H. Arabi [b], A. Shokuhfar [c]

[a] Department of Material Science, Faculty of Engineering, Tarbiat Modares University, Tehran, Iran
[b] Center of Excellence of Advanced Materials and Processing (CEAMP), Department of Materials Science and Engineering, Iran University of Science & Technology (IUST), Tehran, Iran
[c] Department of Material Science, Faculty of Mechanical Engineering, K.N. Toosi University of Technology, Tehran, Iran

ARTICLE INFO

Article history:
Received 2 February 2009
Received in revised form 28 March 2009
Accepted 31 March 2009
Available online 9 April 2009

Keywords:
Aluminum–lithium alloys
DSC
Activation energy
Natural aging
Al–Cu–Li–Zr alloy
T_1 phase
Dissolution energies

ABSTRACT

Guinier–Preston (GP) zone formation and precipitation behavior of T_1 (Al_2CuLi) phase during the aging of an Al–Cu–Li–Zr alloy was studied by differential scanning calorimetry (DSC) technique and electrical resistance measurement of the samples. Results show that precipitation of T_1 phase occurred in temperature range of 250–300 °C whereas its dissolution occurred within the temperature of 450–530 °C. Activation energies for precipitation and dissolution of T_1 phase which were determined for the first time in this research, were 122.1 kJ/mol and 130.3 kJ/mol respectively. Results of electrical resistance measurements showed that an increase in the age hardening time resulted in the reduction of electrical resistance of the samples. In addition, TEM observation showed that T_1 phase has plate shape morphology and its crystal structure is in the form of hexagonal close-packed. The lattice parameters were found to be: $a = 0.4672$ nm and $c = 0.8785$ nm.

1. Introduction

In response to demands of industries for new materials with higher specific modulus and strength, aluminum–lithium alloys were developed. Aluminum–lithium alloys such as 2090, 2091 and 8090 provide higher specific modulus than those of the previous grades of aluminum alloys (e.g. 7075, 2024) and therefore replacements of some parts of aircrafts with these new alloys have been started at the same time [1–5].

Precipitation hardening process is the most important method to improve the mechanical properties of aluminum–lithium alloys. For example, for AA2090 alloy temperature ranges 70–120 °C and 150–210 °C were used respectively for natural and artificial aging in order to improve its mechanical properties [6,7].

The precipitation sequence in AA 2090 alloy represented as: supersaturated solid solution → co-clusters → GP zones → θ'' → θ' → θ → T_1 (Al_2CuLi) [8,9].

High volume fraction of metastable phases such as θ, θ', θ'', T_1, T_2 and T_B are usually formed within the structure of Al–Li 2090 alloy after being subjected to artificial aging processes. In effect, the major phase which has the significant effects on the properties of Al–Li 2090 alloy is said to be T_1 (Al_2CuLi) [10]. T_1 phase has hexagonal lattice and platelet morphology which can be formed during the aging treatments at 135–260 °C.

The orientation relationship between T_1 phase and matrix has been presented by the following equations [11]:

$$(1\,1\,\bar{2}\,0)_{T_1}||(2\,\bar{1}\,\bar{1})_{Al},\quad (0\,0\,0\,1)_{T_1}||$$
$$(1\,1\,1)_{Al},\quad (1\,0\,\bar{1}\,0)_{T_1}||(\bar{1}\,\bar{1}\,0)_{Al}$$

However, activation energies for precipitation and dissolution of the major strengthening phase (i.e. T_1) have not been determined in Al–Cu–Li alloys. Indeed, kinetic of precipitation and dissolution of T_1 phase has not been calculated yet.

Differential scanning calorimetric (DSC) has been effectively used to study phase transformation kinetics in aluminum alloys [12,13]. By fitting a kinetic model to DSC or DIC (Differential Isothermal calorimetry) curves, the kinetic parameters, e.g. the activation energy (E_a) and rate constant (k) can be determined. For linear heating experiments, activation energies of reactions can be derived from a set of DSC experiments which performed at different heating rats (β). Kissinger peak method is widely used to determine activation energies in the reactions when the temperatures of peaks cannot be determined accurately due to overlapping heat effects [12,13].

* Corresponding author. Tel.: +98 261 3505096.
E-mail address: Sh.Ahmadi@modares.ac.ir (S. Ahmadi).

0925-8388/$ – see front matter © 2009 Published by Elsevier B.V.
doi:10.1016/j.jallcom.2009.03.188

In this research, stability of T_1 phase under the different age hardening conditions as well as the effects of GP zones on physical and mechanical properties of an Al–Cu–Li–Zr alloy sheet have been investigated by measuring its hardness, electrical resistant, tensile properties, and evaluating the transmission electron microscopic (TEM) images. Furthermore, for the first time activation energies for precipitation and dissolution of T_1 phase have been determined by performing the DSC experiments at different heating rates.

2. Method and materials

The hot rolled sheet of Al–2.35Cu–2.1Li–0.1Zr (wt.%) alloy with 0.1 wt.% Fe and 0.1 wt.% Si and a thickness of 2 mm was utilized for this investigation. The original sheet was cast, homogenized, and hot rolled in several paths. Then it was solution annealed at 525 °C for one hour and subsequent cold rolled (14% reduction in thickness). Three sets of specimens were prepared from this sheet to the treated under various aging conditions. The first set of the specimens was aged either at 25 °C (natural aging) or at 100 °C after cold rolling. The aging treatments cycles were as follows:

$$\text{Solution annealed} + \text{Natural aged (40 days)} \quad (1)$$

$$\text{S.A.} + \frac{100\,^\circ\text{C}}{100\,\text{h}} \quad (2)$$

The specimens treated by the second cycle, were aged either at 25 °C (natural aging) or at 100 °C prior to aging them at 150 °C for 48 h. The overall aging treatments were:

$$\text{S.A.} + \text{N.A.(40 days)} + \frac{150\,^\circ\text{C}}{48\,\text{h}} \quad (3)$$

$$\text{S.A.} + \frac{100\,^\circ\text{C}}{100\,\text{h}} + \frac{150\,^\circ\text{C}}{48\,\text{h}} \quad (4)$$

The third set of the specimens were aged either at 150 °C or at 190 °C for different times after solution annealing according to the following cycles.

$$\text{S.A.} + \frac{150\,^\circ\text{C}}{6\text{–}100\,\text{h}} \quad (5)$$

$$\text{S.A.} + \frac{190\,^\circ\text{C}}{1\text{–}48\,\text{h}} \quad (6)$$

Discs having dimension of 5 mm diameter and 1 mm thickness were prepared from the sheet mentioned for DSC examination. Scanning of the samples over the temperature rang of 25–1000 °C at three different heating rates of 5, 10 and 15 °C/min were performed in a NEC-409pc calorimeter. Argon was used as both a purge and protective gas during DSC test. Base lines in differential scanning calorimetry tests were determined by not using any sample at all or using "empty pan" method.

Hardness tests were carried out on the aged specimens obtaining from surfaces with #1000 grades Sic-paper. Electrical resistance was measured by a micro-ohmmeter device having 1 μΩ accuracy.

A 200 kV transmission electron microscope (TEM) was applied to determine different precipitates and phases in the structure of the alloy. Before applying microstructural determination, samples were prepared in foil shape with 3 mm diameter. These discs were electropolished in twin jet electropolisher with a solution composed of 25% nitric acid and 75% methanol. It should be noted that electropolishing process was accomplished in −25 °C temperature and DC voltage.

3. Results and discussion

3.1. Properties in low temperature age hardening

Electrical resistance data are very useful tools for studying the initial stages of aging and provide indirect evidence on the interaction between solute atoms and precipitates. Effects of solute atoms on electron scattering are more important than those grain boundaries, dislocation, and precipitates according to Riontino et al. [14] and Gao et al. [15]. Solute atoms, clusters and GP zones disrupt electron flow through the lattice and decrease the conductivity. In Figs. 1 and 2 results of hardness, electrical resistant and tensile tests of the natural and artificial aged samples are shown. Stabilizing of GP zones in the structure of Al–Cu–Li alloy can be claimed in this research because of the increase in the hardness, yield strength and electrical resistant.

3.2. Stability of T_1 phase

Fig. 3 demonstrates the variations in hardness of the alloy at 190 °C and 150 °C for different aging times (second set of the specimens). At aging temperatures of 190 °C and 150 °C, the hardness

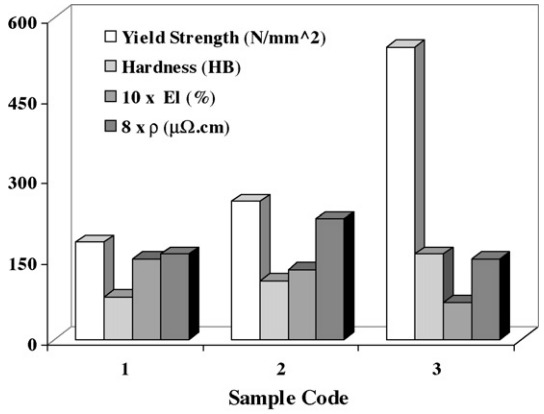

Fig. 1. The effect of heat treatment conditions on variation of hardness; electrical resistance; yield strength and elongation of Al–Cu–Li alloy. Sample code: 1—Solution annealed; 2—Natural aged (40 days); 3—Natural aged (40 days) + aged at 150 °C for 48 h.

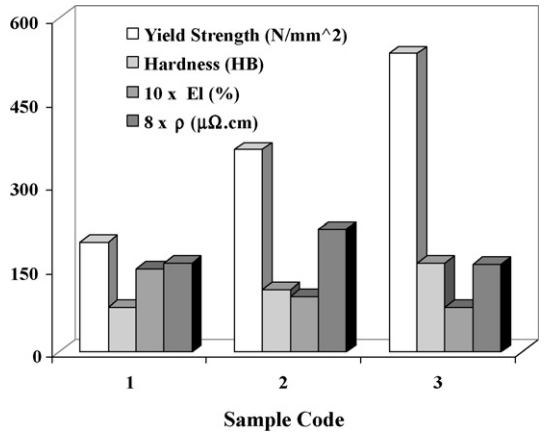

Fig. 2. The effect of heat treatment conditions on variation of hardness, electrical resistance, yield strength and elongation of Al–Cu–Li alloy. Sample code: 1—Solution annealed; 2—Artificial aged 100 °C for 100 h; 3—Artificial aged 100 °C for 100 h + aged at 150 °C for 48 h.

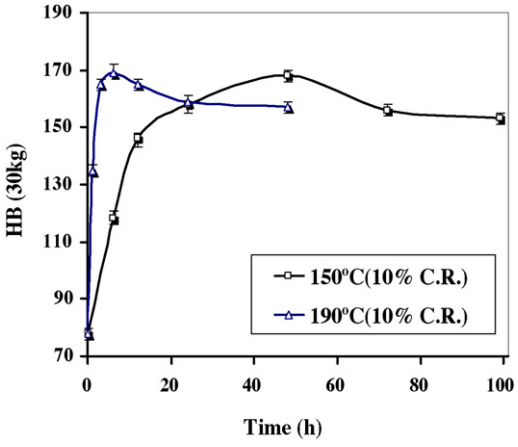

Fig. 3. Relation between hardness and aging time for two different temperatures used for aging treatment.

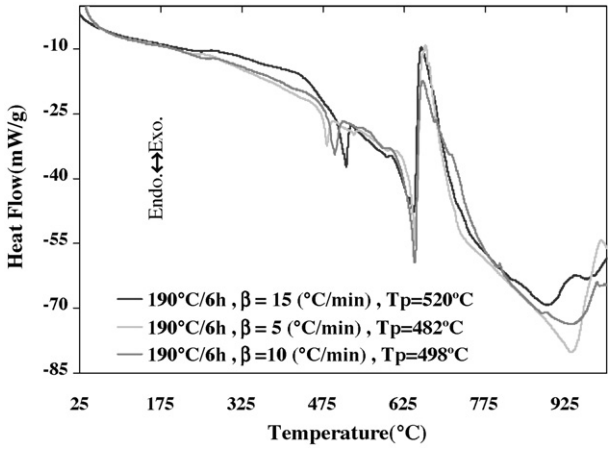

Fig. 4. DSC curves of the specimens aged at 190 °C/6 h in three different heating rates.

gradually increased with the increase of aging time and reached a maximum hardness of 170 HB and 168 HB after 6 h and 48 h aging time respectively. It is clear from the aging curve that at higher temperature over aging occurred in a shorter aging time as expected. This behavior can be attributed to the mechanism of strain hardening in which the dislocation density increased by cold working and thus enhanced the diffusion rate. Therefore, the precipitation rate of alloying elements increased in the microstructure by more dislocation interactions.

It appears that maximum of hardness occurred in the 190 °C/6 h aging condition and therefore this sample was selected for calorimetric studies.

In Fig. 4 result of the calorimetric test of 190 °C/6 h specimen in three different heating rates are shown within which the effects of hating rate on the DSC curves are presented. In all thermograms, main effects consist of: 1-exothermic effect at temperature range of 250–290 °C, 2-endothermic effect at the range of 470–530 °C and 3-endothermic effect at about 610–660 °C. The first peak shows an exothermic reaction that is due to the precipitation or the formation of phases whereas the second peak represents the endothermic effect due to the dissolution of compounds. The main endothermic peaks appeared around 650 °C in DSC curves. In other research, this temperature was attributed to the melting point of AA2090 alloy [16,17]. One also can observe in this figure that by increasing the heating rate, peak of precipitation (T_p^f) shifted from 255 °C to 275 °C while the peak of dissolution (T_p^d) shifted from 482 °C to 520 °C.

Effects of heating rate on precipitation of T_1 phase is presented in Fig. 5. Endothermic effects in the thermograms of Fig. 5 are an indication of dissolution of phases such as T_1, T_2, θ, θ' and

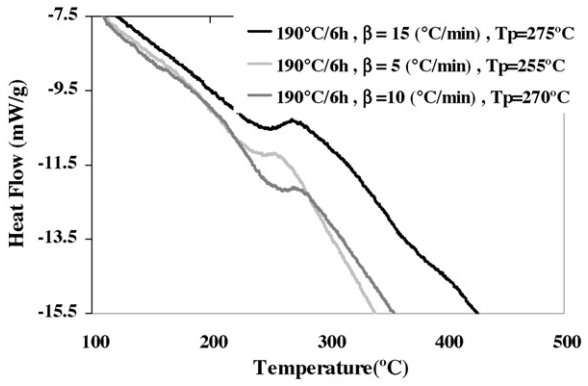

Fig. 5. Variation of T_p^f for three different heating rates.

Table 1
T_p^f for three heating rates measured for the sample aged at 190 °C/6 h.

Heating rate (°C/min)	5	10	15
T_p (°C)	255	270	275

Table 2
T_p^d in three heating rates for 190 °C/6 h aged specimens.

Heating rate (°C/min)	5	10	15
T_p (°C)	482	498	520

T_B. T_1 (Al_2CuLi) phase was the predominant precipitate at temperatures between 135 °C and 260 °C in a similar research [11]. According to the research by Davydov et al. [18], temperature ranges for precipitation and dissolution of T_1 phase in the DSC curves are 275–310 °C and 440–510 °C respectively. Therefore, exothermic effects observed between 250 °C and 300 °C in this research can be attributed to precipitation of T_1 phase. The DSC diagrams at three heating rates show that T_p^f shift to higher temperatures by increasing heating rate (β). In Table 1, the amounts of T_p^f values for three heating rates are given.

Kissinger peak method was used for determination of activation energy in the precipitation and dissolution of T_1 phase. According to Eq. (8), plotting ln (T_p^f/β) versus $1/T_p^f$ gives a straight line, the slope of which equals to E_a/R [15].

$$\ln \frac{T_p^2}{\beta} = \frac{E_a}{RT_P} + C \tag{8}$$

Arrhenius plot for the maximum of the exothermic heat effects has been shown in Fig. 6. Slope of the precipitation line find from this figure was equal to 14.7 and therefore activation energy for the precipitation of T_1 phase was measured to be 122.1 kJ/mol.

Endothermic effects in the temperature range of 450–530 °C in the DSC diagrams were attributed to dissolution of T_1 phase. In Fig. 5 variation of the heat effects for dissolution of T_1 phase (T_p^d) for three different heating rates are shown and Table 2 gives the amounts of T_p^d for the three heating rates. The slop of the line in Arrhenius plot (Fig. 7) for dissolution of T_1 phase was 15.7. Therefore, the activation energy for dissolution of T_1 phase was measured to be 130.3 kJ/mol.

Activation energies observed for precipitation reactions within the temperature range 200–300 °C are closed to the activation energy for diffusion of precipitating elements (this is about 120–135 kJ/mol for Cu, Mg, Si). It is also reported that the activation energies for diffusion of Cu and Li atoms in Al are 135 kJ/mol and 130.1 kJ/mol respectively [13]. In fact, the activation energies obtained for precipitation and dissolution of T_1 phase in this study, i.e. 122.1 kJ/mol and 130.3 kJ/mol, are very close to the activation energies reported for diffusion of alloying elements, i.e. Cu, Li and Mg in Al-base alloys. On the other hand, the results of this research

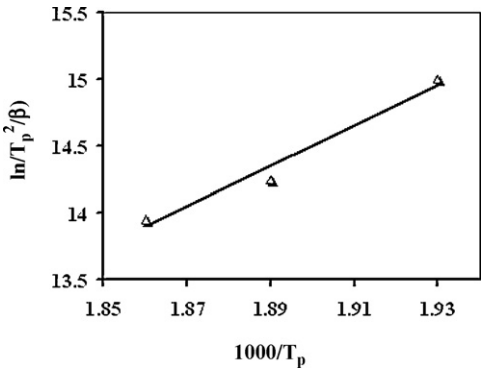

Fig. 6. Arrhenius plot of ln (T_p^2/β) vs 1000/T_P) for precipitation of T_1 phase.

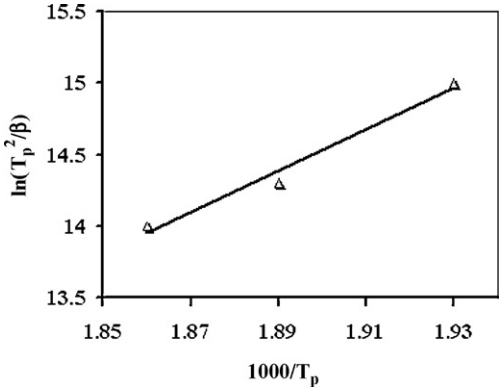

Fig. 7. Arrhenius plot of $\ln(T_p^2/\beta)$ vs $(1000/T_P)$ for dissolution of T_1 phase.

show that the activation energies (calculated from DSC curves) for the precipitation reactions were equal to the activation energies for diffusion of these elements in Al–Cu–Li structure. This is an indication of the stability of some strengthening phases (e.g. T_1) with in the structure of the Al–Cu–Li alloy after the aging processes.

Fig. 8 demonstrates the electrical resistivities of aged specimens for various aging times. This figure indicates that the electrical resistance of the samples decreased during the aging treatments of alloy at both 190 °C and 150 °C. This seems to be due to the formation of the precipitates in the structure during the aging process.

It should be noted here that the maximum of the electrical resistance belonged to the solution heat-treated samples whereas formation of the stable strengthening phases (such as T_1) by aging process caused the electrical resistance to decrease (i.e. electrical conductivity to increase).

3.3. Transmission electron microscopy (TEM) observation

Although there are three kinds of strengthening phases in the structure of Al–Cu–Li alloys (i.e. T_1, T_2, T_B), only $T_1(Al_2CuLi)$ phase has been observed in plate-shaped morphology and hexagonal close-packed (hcp) lattice (Fig. 9) [11]. Microstructure of the alloy is shown in Fig. 10. The most striking feature of the figure is plate - shaped morphology of the precipitated phase. The selected area diffraction pattern (SADP) of the alloy prepared according to 190 °C/6 h aging condition is compatible with hcp lattice. The lattice parameters of the hexagonal precipitate T_1 (i.e. a, c) were calculated by considering the camera constant (λL) and interplanar spacing (d). In principle, a and c were calculated in this research as 0.4672 nm and 0.8785 nm respectively.

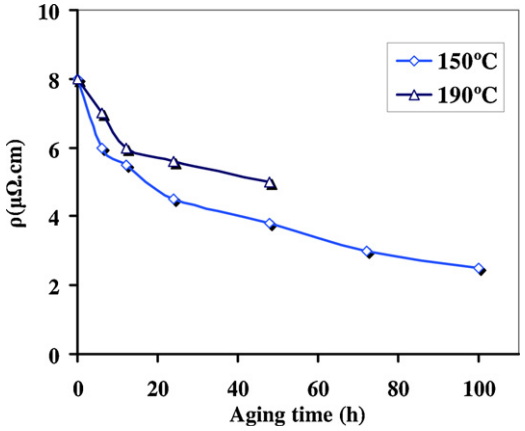

Fig. 8. Relation between electrical resistance and aging time.

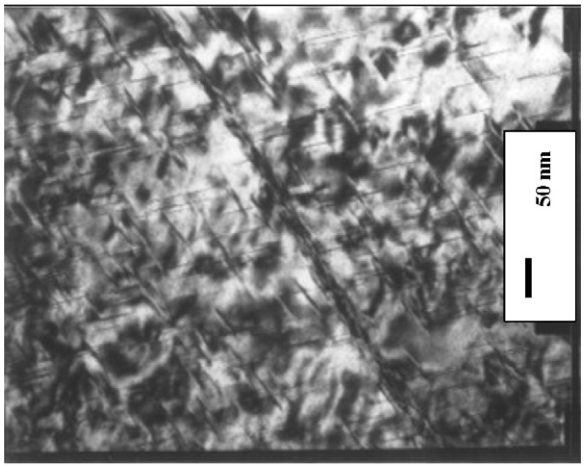

Fig. 9. T_1 phase precipitated in Al–Cu–Li alloy aging at 205 °C for 6 min [11].

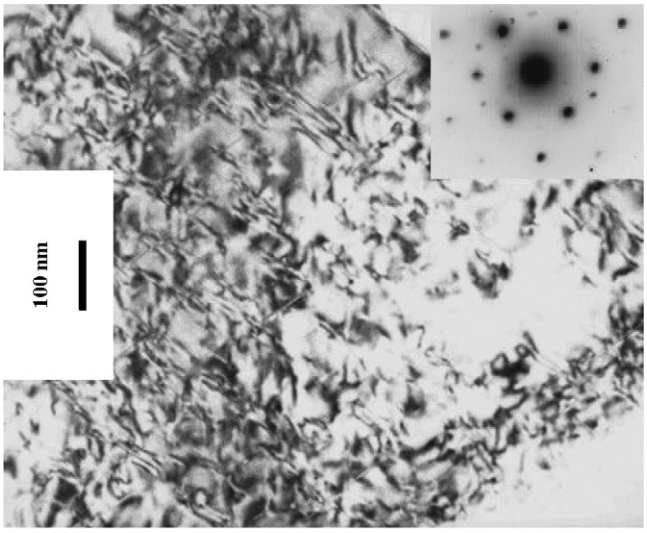

Fig. 10. Microstructure and selected area diffraction pattern of the alloy and precipitated T_1 phase (foil plane was (0 0 0 1) in the TEM observation).

As a matter of fact, differential scanning calorimetric (DSC) evaluation and the TEM observation show that T_1 (Al_2CuLi) phase precipitated in the structure of the Al–Cu–Li alloy due to the strengthening aging treatment.

4. Conclusions

1. Exothermic effects within the temperature range 250–300 °C attributed to the precipitation; and endothermic effects between 450 °C and 530 °C to the dissolution of T_1 phase.
2. Activation energies for the precipitation and the dissolution of T_1 phase were 122.1 kJ/mol and 130.3 kJ/mol respectively. These values are almost equal to the activation energies for diffusion of Cu and Li elements in Al.
3. Low temperature aging process and formation of GP zones in the structure of Al–Cu–Li–Zr alloys increased the electrical resistance apparently by disrupting the electron flow through the lattice. Electrical resistance also decreased by increasing the aging time and temperature. This was probably due to a higher degree of precipitates formation.
4. According to TEM observations, plat-shaped morphology was the most striking feature of the strengthening precipitate in the structure of the alloy.

5. Lattice parameters a and c of the hcp structure of T_1 phase were measured as 0.4672 nm and 0.8785 nm respectively.

Acknowledgements

I am sending an article titled, "Formation Mechanisms of Precipitates in an Al–Cu–Li–Zr Alloy and their Effects on Strength and Electrical Resistance of the Alloy", to be considered for publication in the Journal. This article contains the result of work carried out by the authors. Therefore, unless stated otherwise, the work is original and no part of it has been submitted for publication in any other journal.

References

[1] R.J. Rioja, Mater. Sci. Eng. A 257 (1998) 100–107.
[2] C. Meric, Mater. Res. Bull. 35 (2000) 1479–1494.
[3] J.A. Yurko, SAE Int. (2003) 19.
[4] E.S. Balmuth, R. Schmidt, China, The Metallurgy Society of AIME, in: Second International Aluminum–Lithium Conference, 1983, pp. 70–88.
[5] I.N. Fridlyander, Mater. Sci. Forum 331–337 (2000) 921.
[6] N.I. Kolobnev, L.B. Khokhlatova, I.N. Fridlyander, Mater. Forum 28 (2004) 208–212.
[7] K. Satya, A.A. Gokhale, A.K. Mukhopadhyay, D. Banerjee, D.B. Goel, Mater. Sci. Forum 331–337 (2000) 1043–1048.
[8] A.E. Smith, S. Homolya, Mater. Forum 28 (2004) 139–144.
[9] Y. Nagai, K. Hono, S. Yanagita, T. Honma, Hasegawa, Mater. Forum 28 (2004) 287–292.
[10] F.W. Gayle, B. Vandersande, Acta Mater. 37 (1989) 1033–1046 (No. 4).
[11] P.S. Chen, B.N. Bhat, Alabama, NASA/TM-200-211548, 2002.
[12] J. Yan, M.J. Starink, in: University of Southampton, SO17 IBJ, Materials Research Group, 2004, pp. 31–33.
[13] M.J. Starink:, Int. Mater. Rev. 49 (2004) 191–226.
[14] G. Riontino, S. Abis, Mengucci, Mater. Sci. Forum 331–337 (2000) 1025–1030.
[15] N. Gao, M.J. Starink, L. Davin, Mater. Sci. Technol. 21 (2005) 1010–1018.
[16] A. Gaber, K. Matsuda, Z. Yong, T. Kawabata, A.M. Ali, S. Ikeno, Mater. Forum 28 (2004) 402–405.
[17] L. Davin, A. Cerezo, N. Gao, M.J. Statink, Surf. Interface Anal. 36 (2004) 589–593.
[18] V.G. Davydov, J.N. Fridlyander, M.V. Samarina, A.I. Orozov, L.B. Ber, Mater. Sci. Forum 331–337 (2000) 1049–1054.